Available online at www.sciencedirect.com

ScienceDirect

journal homepage: www.elsevier.com/locate/bbe

Original Research Article

Robust and accurate optic disk localization using vessel symmetry line measure in fundus images

Rashmi Panda *, *Puhan N.B.*, *Ganapati Panda*

School of Electrical Sciences, Indian Institute of Technology Bhubaneswar, India

ARTICLE INFO

Article history:
Received 8 February 2017
Received in revised form
16 May 2017
Accepted 22 May 2017
Available online 31 May 2017

Keywords:
Optic disk localization
Symmetry
Glaucoma
Diabetic retinopathy
Computer-aided diagnosis

ABSTRACT

Accurate optic disk (OD) localization is an important step in fundus image based computer-aided diagnosis of glaucoma and diabetic retinopathy. Robust OD localization becomes more challenging with the presence of common pathological variations which could alter its overall appearance. This paper presents a novel OD localization method by incorporating salient visual cues of retinal vasculature: (1) global vessel symmetry, (2) vessel component count and (3) local vessel symmetry inside OD region. In the proposed method, a new vessel symmetry line (*VSL*) measure is designed to demarcate the lines that divide the retinal vasculature into approximately similar halves. The initial OD center location is computed using the highest number of major blood vessel components in the skeleton image. The final OD center localization involves an iterative center of mass computation to exploit the local vessel symmetry in the OD region of interest. The proposed method shows effectiveness in diseased retinas having diverse symptoms like bright lesions, hemorrhages, and tortuous vessels that create potential ambiguity for OD localization. A total of ten publicly available retinal image databases are considered for extensive evaluation of the proposed method. The experimental results demonstrate high average OD detection accuracy of 99.49%, while achieving state-of-the-art OD localization error in all databases.

1. Introduction

Optic disk (OD) localization is an important aspect of fundus image analysis in computer-aided diagnosis of glaucoma and diabetic retinopathy [1]. The optic disk appears as a bright and relatively circular structure in normal fundus images (Fig. 1). Accurate OD localization ensures efficient optic disk and cup segmentation which is crucial for deriving cup-disk-ratio (CDR) based glaucoma risk index [2]. In diabetic retinopathy affected images, the optic disk region can be easily confounded with the bright exudates. Hence, the optic disk is identified and discarded to enhance the exudate detection performance [3]. Moreover, OD also acts as a landmark in the localization of fovea and macula [4].

Various methods have been proposed in the literature for OD localization using retinal anatomical structures. The methods can be broadly grouped in two categories, i.e. appearance based methods and model based methods. The appearance based methods are designed based on the shape

* *Corresponding author at*: School of Electrical Sciences, Indian Institute of Technology Bhubaneswar, India.
E-mail addresses: rp14@iitbbs.ac.in (R. Panda), nbpuhan@iitbbs.ac.in (P. N.B.), gpanda@iitbbs.ac.in (G. Panda).

http://dx.doi.org/10.1016/j.bbe.2017.05.008

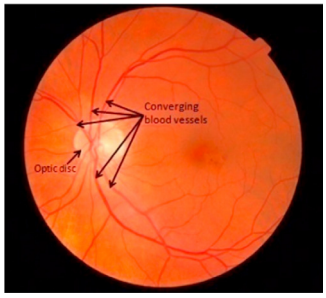

Fig. 1 – Healthy retina containing bright and circular OD with converging blood vessels.

and brightness characteristics of OD. Sinthanayothin et al. proposed a method based on the fact that the OD has the highest image variance due to the bright OD pixels and the dark retinal blood vessel pixels within the OD region [4]. Walter and Klein detected the OD assuming that OD is the brightest region within a retinal image [5]. Multiple line operators in specific directions are designed by Lu and Lim to capture circular brightness structures [6]. The effectiveness of the appearance based methods is reduced in images having non-uniform illumination and pathological images causing changes in OD appearance due to the interference of large exudates and bright artifactual features.

It is observed that blood vessels are most stable anatomical structures in the pathological fundus images (Fig. 2). Thus, model based OD localization techniques which uses blood vessel map tend to be more reliable even in the presence of retinal pathologies. Hoover and Glodbaum exploited the fuzzy convergence property of blood vessels at the OD center [7]. This method reported an overall accuracy of 89% and several failure cases arise due to the convergence of vessels around a bright lesion. OD is localized as the common vertex of two parabolas fitted with the major blood vessels in [8]. Youssif et al. developed an OD detection algorithm based on matched filtering which matches the directional pattern of the retinal blood vessels [9]. Mahfouz and Fahmy identified the OD by locating the peak of the 1-D projections with an accuracy of 92.59% [10]. The working parameters of [8], the filters of [9], size of the projection windows of [10] need to be tuned separately for different databases. Circular transformation is used to locate the OD based on its shape and image variations across the OD boundary in [11]. The images having very low image variation across the OD boundary reported incorrect OD localization in this method.

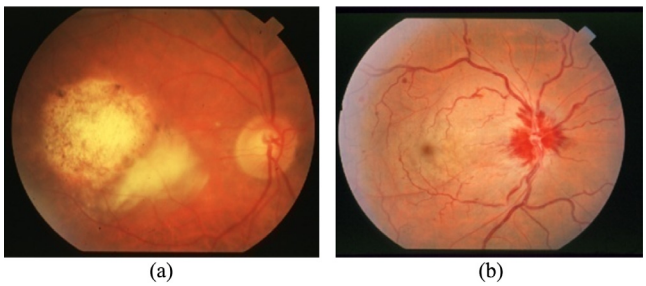

Fig. 2 – (a) Retinal image having lesions of higher brightness and larger size than OD. (b) Retinal image where OD is completely covered by hemorrgages.

Welfer et al. [12] proposed a new adaptive method for automatic localization and segmentation of the optic disk using mathematical morphology. Soares et al. [13] performed OD localization based on the cumulative sum field computed from retinal vessel orientations. This method reports an average accuracy of 99.15%. Zhang and Zhao suggested an OD detection method based on vessel distribution and directional characteristics along with global Hough transform [14]. Main limitations of the model based methods are that they are complex and require high computation time. Moreover, complete and accurate vasculature favors the model based techniques, since very high detection accuracy is achieved when manually labeled vessels are utilized. Giachetti et al. applied fast radial symmetry transform as the principal cue to locate optic disk centers and reported high detection accuracy of 99.66% in MESSIDOR database [35]. Bekkers et al. proposed a template matching approach to recognize a curved geometry on the position-orientation domain [36]. Dashtbozorg et al. presented an automatic approach for OD center detection and segmentation using a multiresolution sliding band filter (SBF) which is suitable for the enhancement of bright circular regions [37].

In this paper, we propose a robust and accurate approach for OD localization by incorporating three salient visual cues derived from retinal vasculature symmetry and convergence characteristics. Our contribution in the paper can be summarized as follows: first, we explore the global symmetry of the segmented vessel map to select lines which divides it into approximately similar halves. Second, we observe that highest number of major blood vessel components converge inside the OD region (vessel component count). We formulate an algorithm to locate the initial OD center on the global symmetry line by designing two semi-annular masks. Third, despite the fact that the retinal blood vessels usually exhibit a random pattern in fundus images [15], we observe local symmetry and dense vessel distribution inside the OD region. This visual cue helps us to detect the final OD center location by an iterative computation of center of mass. The proposed method's performance is evaluated by using 10 publicly available databases such as DRIVE, STARE, HRF, ROC, E-OPHTHA-EX, DIARETDB0, DIARETDB1, MESSIDOR, DRIONS-DB, and DRISHTI-GS. The high average detection accuracy of 99.49% is achieved despite the presence of large number of pathological fundus images. Further, the parameters used in the method are simple to select and they are consistent for the fundus images in all databases.

The organization of the paper is as follows: The proposed OD localization method is formulated in Section 2. The materials used for evaluation of the proposed method and analysis of the obtained results are discussed in Section 3. Finally, some concluding remarks are noted in Section 4.

2. Proposed optic disk localization method

For OD localization, we have selected the green channel (Fig. 3 (a)) of the RGB color image (Fig. 2(a)) as it provides best contrast and clinical information of retinal structures. The proposed OD

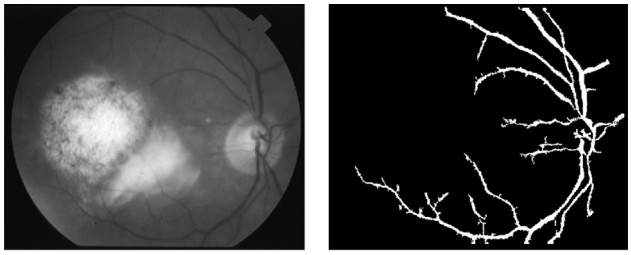

Fig. 3 – (a) Green channel image of Fig. 2(a). (b) Corresponding major blood vessel map.

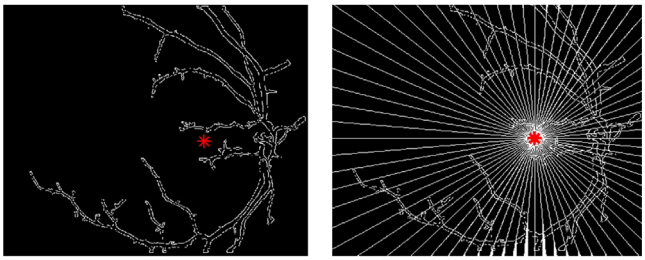

Fig. 4 – (a) The CM pixel of I_{edge} is marked as '*'. (b) All evenly oriented radial lines passing through the CM pixel.

localization method is divided into three parts: (1) Vessel symmetry line selection which divides the major blood vessel into two similar halves (Section 2.1); (2) Initial OD center detection using highest vessel component count (Section 2.2); (3) final OD center localization using iterative center of mass computation (Section 2.3). A preliminary version of the proposed method can be found in [18].

2.1. *Vessel symmetry line selection*

The new vessel symmetry line (*VSL*) measure is designed based on the facts that major (thick) blood vessels converge at the OD center and the vessel map is associated with global symmetry. Here, we suggest a new algorithm to compute the *VSL* measure which enables us to detect the global symmetry lines. Prior to symmetry line detection, the blood vessel map is obtained using an existing segmentation algorithm [16]. However, other vessel segmentation algorithms available in the literature can also be applied for this purpose [17,34]. The major vessels ($I_{BVmajor}$) are retained from the vessel map after using the morphological erosion operator (Fig. 3(b)). The finer blood vessels are not considered while determining the *VSL* measure as they have a random pattern which might create perplexity. We consider only the edges (I_{edge}) of the major blood vessel map while designing the *VSL* measure to reduce the computational complexity.

In I_{edge}, we consider N evenly oriented radial lines (L_θ) passing through the center of mass (*CM*) at angle θ with the horizontal. The *CM* coordinate (r_{cm}, c_{cm}) of I_{edge} is computed as

$$(r_{cm}, c_{cm}) = \left(\frac{\sum_{i=1}^{P} r_{edge}(i)}{P}, \frac{\sum_{i=1}^{P} c_{edge}(i)}{P} \right) \tag{1}$$

where (r_{edge}, c_{edge}) represent the edge pixel coordinates and P represents the total number of edge pixels (Fig. 4(a)).

Each L_θ divides I_{edge} into two similar halves $I_{half1\_L_\theta}$ and $I_{half2\_L_\theta}$. The orientation θ is varied from 0 to π with an interval of α°. Here we choose $\alpha = 5^\circ$ and thus the total number of lines is equal to 36 $(N = \pi/\alpha)$ which are drawn in Fig. 4(b). It can be observed that any L_θ, which can divide the blood vessel into the halves having similar distribution, passes through/near the OD region. To quantify this visual symmetry for selecting the symmetry line L_θ, we employ the partial Hausdorff distance (*PHD*) measure.

2.1.1. *Partial Hausdorff distance measure*

Partial Hausdorff distance (*PHD*) is designed as a dissimilarity measure defined on the point sets [19,20]. Let $A = \{a_1, a_2, \ldots, a_m\}$ and $B = \{b_1, b_2, \ldots, b_n\}$ be the point sets. Then, the *PHD* measure between the sets A and B is defined as

$$PHD(A,B) = \max(h_p(A,B), h_p(B,A)) \tag{2}$$

where h_p is the directed partial Hausdorff given by

$$h_p(A,B) = R^{\text{th}} \min_{a \in A, b \in B} \|a_i - b_i\|. \tag{3}$$

In Eq. (3), $\|\cdot\|$ represents the norm of the vector. $h_p(A,B)$ and $h_p(B,A)$ are directed *PHD*s from A to B and from B to A respectively. The *PHD* considers the R^{th} ranked maximum value instead of the overall maximum as in the conventional directed Hausdorff distance [21]. The $PHD(A,B)$ is then the maximum of the directed distances.

The conventional Hausdorff was applied for similarity comparison of visual objects [21]. When a part of the object is missing or in the presence of outliers or occlusion, the conventional Hausdorff dissimilarity becomes undesirably large in object matching. Hence, a modified *PHD* measure is proposed for such scenario in [19]. The retinal blood vessels in individual retina have unique random distribution and $I_{half1\_L_\theta}$, $I_{half2\_L_\theta}$ may not be exactly the same. Thus, considering the above mentioned advantages of the *PHD* measure, we decide to apply partialness with Hausdorff operator in our symmetry measure formulation.

2.1.2. *VSL measure*

The vessel distribution on both sides of an accurate symmetry line L_θ appears to be similar (Fig. 5). Thus, the edge pixels found on the line L_{θ_ortho} (orthogonal to L_θ at p_m) should be more or less equidistant to each other. Let the distance values of the edge pixels on L_{θ_ortho} in $I_{half1\_L_\theta}$ and $I_{half2\_L_\theta}$ form two sets $set1_{p_m}$ and $set2_{p_m}$ respectively.

Mathematically,

$$p_m = \text{pixel on the line } L_\theta, \quad m = 1, 2, \ldots, M \tag{4}$$

$$set1_{p_m} = \{d_{11}, d_{12}, \ldots, d_{1j}\} \tag{5}$$

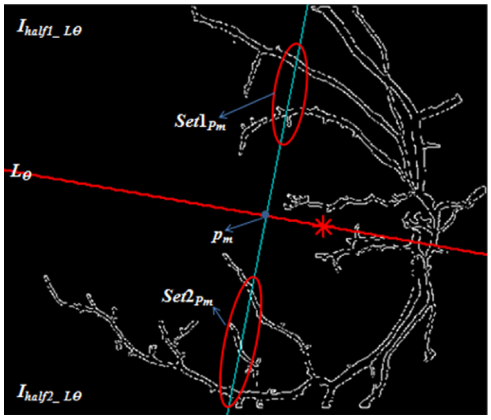

Fig. 5 – The illustration of formation of $set1_{p_m}$ and $set2_{p_m}$.

$$set2_{p_m} = \{d_{21}, d_{22}, \ldots, d_{2k}\} \quad (6)$$

Here, M represents the total number of pixels on L_θ, d_{1j} and d_{2k} are the distances of j^{th} and k^{th} edge pixels from p_m present in $I_{half1\_L_\theta}$ and $I_{half2\_L_\theta}$ respectively.

The similarity between the two sets $set1_{p_m}$ and $set2_{p_m}$ for each pixel p_m is computed using the *PHD* measure, which is denoted by $PHD_{p_m}(set1_{p_m}, set2_{p_m})$. The *VSL* measure for L_θ is found as the mean of all PHD_{p_m} values computed at each pixel of L_θ.

$$VSL_\theta = \frac{\sum_{m=1}^{M} PHD_{p_m}}{M} \quad (7)$$

We select K lines $[L_{\theta 1}, L_{\theta 2}, \ldots, L_{\theta K}]$ having the least VSL_θ values as symmetry lines out of N radial lines. It can be observed that three symmetry lines pass through/near OD in Fig. 6. The process of symmetry line selection is summarized in Algorithm 1.

Algorithm 1. Vessel symmetry line (*VSL*) measure computation

Input: Green channel fundus image I_G
Output: K symmetry lines $[L_{\theta 1}, L_{\theta 2}, \ldots, L_{\theta K}]$

- Obtain $I_{BVmajor}$ and I_{edge} using [19].
- Find center of mass (r_{cm}, c_{cm}) of I_{edge} using (1).
- Define the line L_θ that passes through (r_{cm}, c_{cm}) and making an angle θ with the horizontal in I_{edge}, where
  $\theta = n\alpha, \quad \forall n = \{0, 1, 2, \ldots, \frac{\pi}{\alpha}\}$
- **For** the line L_θ
  For each point $p_m$on L_θ, $\forall\, m = 1, 2, 3, \ldots, M$
  $set1_{p_m} = \{d_{11}, d_{12}, \ldots, d_{1j}\}$
  $set2_{p_m} = \{d_{21}, d_{22}, \ldots, d_{2k}\}$
  where, $set1_{p_m}$ and $set2_{p_m}$ contains the distance values of the edge pixels situated on L_{θ_ortho}.
  find $PHD_{p_m}(set1_{p_m}, set2_{p_m})$ using (2)
  end
  $VSL_\theta = \frac{\sum_{m=1}^{M} PHD_{p_m}}{M}$
  end
- Find K minimum VSL_θ values. The corresponding lines $[L_{\theta 1}, L_{\theta 2}, ..L_{\theta K}]$ are the symmetry lines.

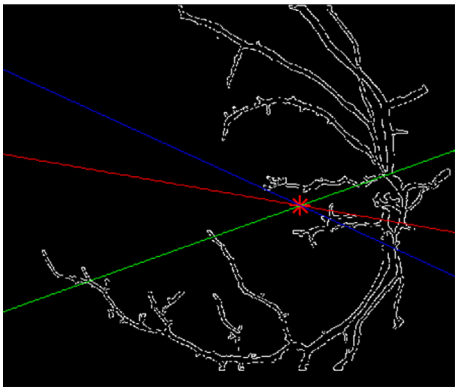

Fig. 6 – Three symmetry lines $[L_{\theta 1}, L_{\theta 2}, L_{\theta 3}]$ shown as red, blue and green lines respectively.

2.2. Initial OD center computation

In this section, the initial OD center is identified on the symmetry lines by defining the vessel component count. The number of major blood vessel components converging around the OD center is more than any other location in the fundus image. This property exists in many fundus images irrespective of the health of the retina. The vessel component count (*VCC*) is defined using two semi-annular masks centered on each pixel of the symmetry lines. The individual vessel components are obtained by generating the skeleton image of $I_{BVmajor}$. On the symmetry lines, the pixel having maximum *VCC* indicates the initial location of OD center.

In certain macula-centered fundus images, the blood vessels bend towards the macula or comparatively more vessel branching are observed. False OD may be detected in such cases when *VCC* is computed using single annular mask. To tackle this situation, we design two semi-annular masks with appropriate radii. When the fundus image is macula-centered or OD-centered, a high number of vessel components is observed in either of the semi-annular masks positioned on the actual OD center. On the other hand, significantly less vessel components are included in the semi-annular masks at non-OD center locations.

The semi-annular masks SM_{left} and SM_{right} of inner radius (r_1) and outer radius ($r_2 = 2r_1$) are shown in Fig. 7. The radii r_1 and r_2 are chosen such that the semi-annular rim remains outside the OD. If larger r_1 is considered, then the mask will

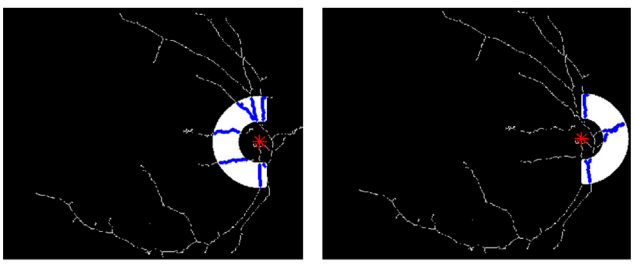

Fig. 7 – (a, b) Semi-annular masks SM_{left} and SM_{right} with blood vessel components, when overlapped on the skeleton image of $I_{BVmajor}$.

contain secondary vessel branches leading to inaccurate vessel component count. On the other hand, when r_1 is very small, the mask may not include the converging blood vessel components. Thus, the optimum value of r_1 is chosen to be slightly more than the OD radius.

The vessel component count (VCC_{sk}) for s^{th} pixel on k^{th} symmetry line is given by

$$VCC_{sk} = \max(VCC_{sk}^{SM_{left}}, VCC_{sk}^{SM_{right}}), \quad s = 1, 2, ..., M \tag{8}$$

where $VCC_{sk}^{SM_{left}}$ and $VCC_{sk}^{SM_{right}}$ denote the vessel component counts using SM_{left} and SM_{right} respectively. Initial OD center is found as

$$S = \arg\max_{s}(VCC_{sk}), \quad k = 1, 2, ...K. \tag{9}$$

The initial OD center coordinates detected on the symmetry line is shown in Fig. 8. The process of initial OD center computation is described in Algorithm 2.

Algorithm 2. Initial OD center computation

Input: Blood vessel map I_{BV},
The K symmetry lines $[L_{\theta 1}, L_{\theta 2}, \ldots, L_{\theta K}]$
Output: Initial OD location S
For each $L_{\theta k}$, $\forall\, k = 1, 2, \ldots, K$
For point p_{sk} on $L_{\theta k}$, $\forall\, s = 1, 2, 3, \ldots, M$
find $VCC_{sk}^{SM_{left}}$ and $VCC_{sk}^{SM_{right}}$ on p_{sk}
$VCC_{sk} = \max(VCC_{sk}^{SM_{left}}, VCC_{sk}^{SM_{right}})$
end
end
$S = \arg\max_s(VCC_{sk}), \quad k = 1, 2, \ldots, K$

2.3. *Final OD center localization*

The final step of the proposed method is based on the local vessel symmetry observed in the vicinity of OD center. The center of mass (CM) of the symmetric vessel map inside the OD region will be situated very close to the actual OD center. We compute the CM of the blood vessel pixels inside a circle of radius r_1 centered on S. If the symmetry line passes slightly away from the OD region, more iterations become necessary till convergence is achieved.

$$S_{i+1} = \left\{ CM_{s_i}^{r_1}(I_{BVmajor}) | \|S_{i+1} - S_i\| \leq \epsilon \right\} \tag{11}$$

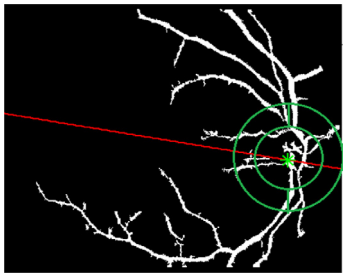

Fig. 8 – The pixel having maximum vessel component count is '*'marked on the symmetry line.

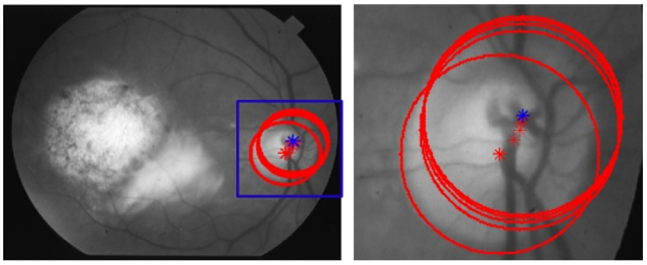

Fig. 9 – (a) Iterative computation for OD center localization. (b) Enlarged (inset) OD portion.

where S_i and S_{i+1} are OD centers in two consecutive iterations, $CM_{s_i}^{r_1}(I_{BVmajor})$ denotes the CM of blood vessel pixels inside circle of radius r_1 centered on S_i and ϵ denotes the threshold for convergence. The iterative process of OD center localization is illustrated in Fig. 9. The final OD center computation is given in Algorithm 3.

Algorithm 3. Final OD center localization

Input: Initial OD location S
Output: Final OD center location S_{final}
- Initialization step
  $i = 1$, $S_i = S$, $S_{i+1} = 0$
- **if** $(|S_{i+1} - S_i| > \epsilon)$
  S_{i+1} = CM of blood vessel pixels inside the circle of radius r_1 centered on S
  $i = i + 1$
  else
  $S_{final} = S_{i+1}$
  end

3. Results and discussion

In this section, the performance of the newly proposed method is extensively evaluated using 10 publicly available retinal databases containing pathological images. The description of each database used for OD localization, results and discussion is presented in the following.

3.1. *Fundus image databases*

A total of ten publicly available databases containing a total of 1978 images considered for evaluation are: DRISHTI-GS [22], DRIONS-DB [23], E-OPHTHA-EX [24], MESSIDOR [25], DIARETDB1 [26], DIARETDB0 [27], DRIVE [28], HRF [29], ROC [30], STARE [31]. Only HRF database provided OD center groundtruth. For other databases the OD centers (groundtruth) are manually annotated and verified by experts from a local eye hospital. The imaging modalities and relevant information regarding the databases are provided in Table 1.

For a given retinal image, the OD localization error is computed as the Euclidean distance between the detected OD center and groundtruth. For whole database, the OD localization error is found by taking the mean and standard deviation

Table 1 – Description of the publicly available retinal databases and scale factors used in the proposed method.

Database	No. of images (normal/diseased)	Camera	Original image dimension	FOV	Scaled image dimension	Scale factor
DRISHTI-GS [22]	101(31/70)	–	2047 × 1760	30°	670 × 577	0.33
DRIONS-DB [23]	110 (0/110)	Color analogical fundus camera	600 × 400	–	600 × 400	1
E-OPTHA-EX [24]	82 (35/47)	–	2544 × 1696, 2048 × 1300, 1440 × 960	40°	848 × 565, 682 × 433, 700 × 480	0.33, 0.33, 0.5
MESSIDOR [25]	1200 (546/654)	Topcon TRC NW6	2240 × 1488, 2340 × 1536, 1440 × 960	45°	746 × 496, 780 × 512, 700 × 480	0.33, 0.33, 0.5
DIARETDB1 [26]	89 (5/84)	Nikon F5	1500 × 1152	50°	750 × 576	0.5
DIARETDB0 [27]	130 (20/110)	–	1500 × 1152	50°	750 × 576	0.5
DRIVE [28]	40 (33/7)	Canon CR5	564 × 584	45°	564 × 584	1
HRF [29]	45 (15/30)	Canon CR1	3504 × 2336	45°	876 × 584	0.25
ROC [30]	100	Topcon NW 100, Canon NW 200, CanonCR5	768 × 576, 1394 × 1392	–	768 × 576, 697 × 696	1, 0.5
STARE [31]	81 (31/50)	Topcon TRV-50	605 × 700	35	605 × 700	1

of individual errors. The OD localization is inferred being accurate if the OD center is positioned within 60 pixels distance from the groundtruth. This evaluation approach for computing both accuracy and OD localization error is adopted from the existing techniques in [7–10,13].

3.2. OD localization results

The fundus image dimension varies across the databases. To maintain the coherence of parameters among the databases, images with higher dimension are scaled down using bicubic interpolation without affecting the aspect ratio [6,11,13,14]. The image dimension after scaling and the scale factors are given in Table 1. A total of four parameters (α, K, r_1 and r_2) are experimentally selected in the proposed method to maximize its performance and they are consistent for all test images. The value of bin angle α is determined as 5°. Three vessel symmetry lines $[L_{\theta 1}, L_{\theta 2}, L_{\theta 3}]$ ($K = 3$ in Eq. (8)) are chosen such that at least in one case the symmetry line passes near the actual OD center. The radii r_1 and r_2 are chosen such that the semi-annular mask remains outside the OD region. In our method, we have found $r_1 = 65$ and $r_2 = 2 \times r_1 = 130$ pixels.

A small deviation in selecting the value of r_1 does not significantly affect the OD localization accuracy. To validate this, we have randomly selected 30 images (3 images from each database) and computed the localization error for different values of r_1 (55, 60, 65, 70 and 75). The localization error in each image for different values of r_1 is plotted Fig. 10(a). The mean localization error of all images for each value of r_1 plotted in Fig. 10(b). It can be verified from both plots that the localization error does not get significantly affected with respect to r_1.

To check the robustness of proposed method against the distortion in pathological images, we select few challenging images from different databases in Fig. 11. In Fig. 11(a)–(d), OD is neither bright nor circular. In Fig. 11(e)–(i), bright lesions which are larger and brighter than the OD are present. Fig. 11 (j)–(l) contain multiple bright spots around OD region. Appearance based methods [4–6] tend to result failures for these scenarios. It is also challenging for [8,12], which use

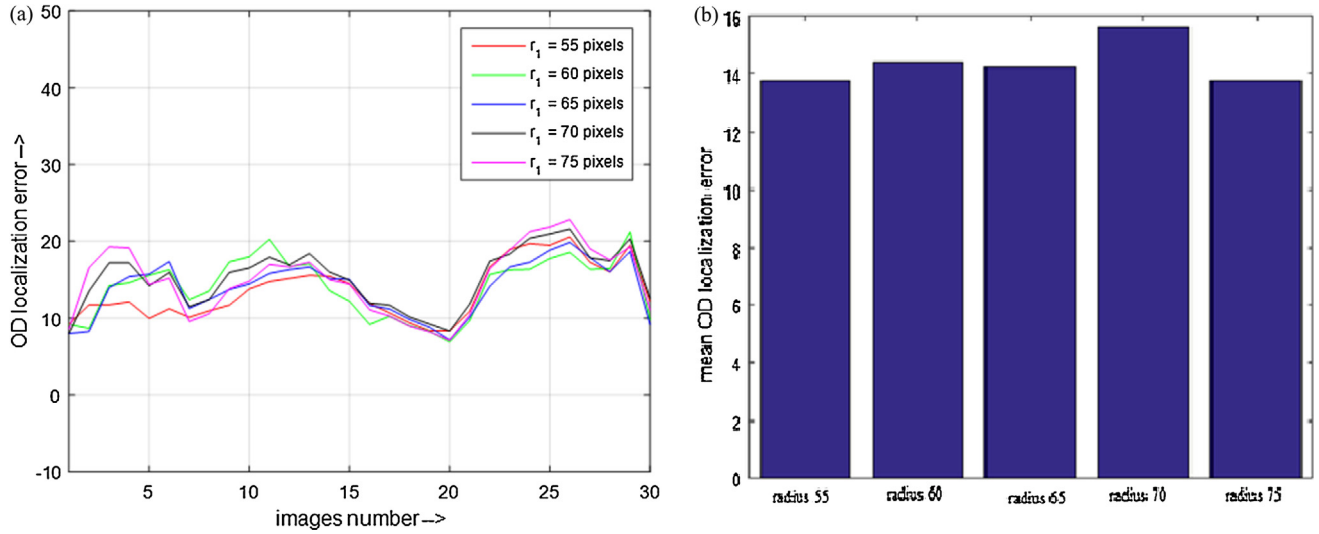

Fig. 10 – (a) OD localization error for 30 test images with different values of r_1. (b) mean localization errors for five radii values.

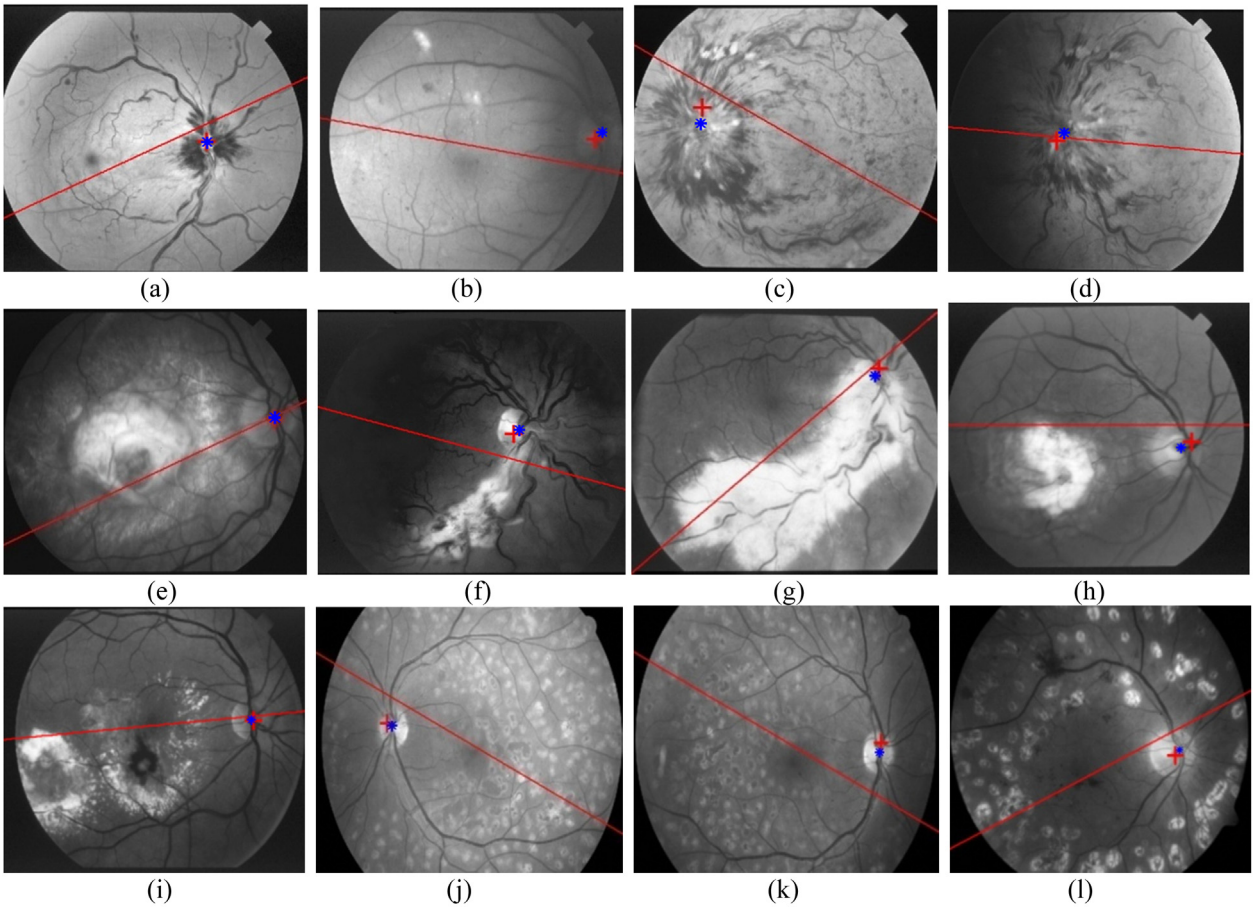

Fig. 11 – (a–l) Accurate OD localization in pathological images suffering from different types of lesions and imaging artifacts. Detected OD center is labeled with "+", groundtruth is labeled as '*' and the corresponding symmetry line is plotted.

convergence of blood vessel and morphological operations, to detect the correct OD location in Fig. 11(a), (c), (d), and (g) as the blood vessel pattern is affected by pathology. However, it can be observed that despite such challenges, the new method is able to accurately locate the OD center in these test images. This is because we explored the symmetric pattern of segmented vessel map through the *VSL* measure along with converging blood vessel components (*VCC*) and iterative center of mass computation. Moreover, our algorithms do not need to search over whole image space to detect the OD. The final OD center is searched only in the vicinity of selected symmetry lines which reduces computational complexity.

The performance comparison of accuracy, number of failure cases and OD localization error in different databases are given in Tables 2–10. The OD localization error in the proposed method is computed by considering the initial size conditions. After detecting the OD location in the resized image by the proposed method, the image is again rescaled to the original resolution. Then the OD localization error is computed as the distance between the groundtruth and detected OD center location in the original resolution. A similar approach was followed by Soares et al. [13]. The performance of the existing methods are obtained from the literature, evaluated on the common databases.

The normalized localization error is computed by dividing the distance between the detected OD center and the groundtruth with the expected OD radius for that image, which is estimated from the image acquisition parameters [35]. The normalized localization error is an effective measure when the image resolution is non-uniform in a database as in MESSIDOR. In MESSIDOR database, the average value of the normalized OD localization error using the proposed method is computed to be 0.121, which is comparable to Giachetti et al. (0.118) [35].

The proposed method achieves 100% correct OD detection accuracy in DRISHTI-GS and DRIONS-DB databases (Table 2).

Table 2 – OD localization accuracy for new databases.

Database	Accuracy (%)	Number of failed images	OD localization error (mean ± std. deviation)
DRISHTI-GS [22]	100	0	38.04 ± 14.51 pixels
DRIONS-DB [23]	100	0	18.63 ± 20.89 pixels

Table 3 – Comparison of OD localization accuracy in E-OPTHA-EX database.

Methods	Accuracy (%)	Number of failed images	OD localization error (mean ± std. deviation)
Soares et al. [13]	99	1	34.62 ± 29.60 pixels
Proposed method	100	0	24.78 ± 11.90 pixels

Table 4 – Comparison of OD localization accuracy in MESSIDOR database.

Methods	Accuracy (%)	Number of failed images	OD localization error (mean ± std. deviation)
Lu and Lim [6]	99.75	3	–
Aquino et al. [32]	98.83	14	–
Ramakanth and Babu [33]	99.42	7	–
Soares et al. [13]	99.25	9	24.59 ± 17.24 pixels
Giachetti et al. [35]	99.16	10	–
Bekkers et al. [36]	99.9	1	–
Proposed method	99.75	3	21.81 ± 12.8 pixels

Table 5 – Comparison of OD localization accuracy in DIARETDB1 database.

Methods	Accuracy (%)	Number of failed images	OD localization error (mean ± std. deviation)
Welfer et al. [12]	97.75	2	–
Mahfouz and Fahmy [10]	97.75	2	–
Lu and Lim [6]	98.88	1	–
Zhang and Zhao [14]	100	0	–
Soares et al. [13]	98.88	1	24.08 ± 14.87 pixels
Proposed method	100	0	22.15 ± 16.43 pixels

Table 6 – Comparison of OD localization accuracy in DIARETDB0 database.

Methods	Accuracy (%)	Number of failed images	OD localization error (mean ± std. deviation)
Mahfouz and Fahmy [10]	98.46	2	–
Lu and Lim [6]	99.23	1	–
Soares et al. [13]	98.46	2	23.51 ± 17.57 pixels
Proposed method	96.92	4	25.84 ± 17.68 pixels

Table 7 – Comparison of OD localization accuracy in DRIVE database.

Methods	Accuracy (%)	Number of failed images	OD localization error (mean ± std. deviation)
Youssif et al. [9]	100	0	17 pixels
Welfer et al. [12]	100	0	11 ± 11 pixels
Mahfouz and Fahmy [10]	100	0	–
Lu [11]	97.5	1	–
Zhang and Zhao [14]	100	1	–
Soares et al. [13]	100	0	14.33 ± 9.77 pixels
Bekkers et al. [36]	97.8	1	–
Proposed method	100	0	16.4 ± 11.5 pixels

Table 8 – Comparison of OD localization accuracy in HRF database.

Methods	Accuracy (%)	Number of failed images	OD localization error (mean ± std. deviation)
Soares et al. [13]	100	0	48.85 ± 22.26 pixels
Proposed method	100	0	49.14 ± 19.34 pixels

Table 9 – Comparison of OD localization accuracy in ROC database.

Methods	Accuracy (%)	Number of failed images	OD localization error (mean ± std. deviation)
Soares et al. [13]	99	1	23.93 ± 14.95 pixels
Proposed method	99	1	24.16 ± 13.27 pixels

Table 10 – Comparison of OD localization accuracy in STARE database.

Methods	Accuracy (%)	Number of failed images	OD localization error (mean ± std. deviation)
Foracchia et al. [8]	97.53	2	23 pixels
Youssif et al. [9]	98.77	1	26 pixels
Hoover and Goldbaum [7]	88.89	9	29 pixels
Mahfouz and Fahmy [10]	92.59	6	14 ± 15 pixels
Lu and Lim [6]	96.30	3	25pixels
Lu [11]	98.77	1	6 pixels
Zhang and Zhao [14]	98.77	1	–
Soares et al. [13]	98.77	1	18.28 ± 12.78
Bekkers et al. [36]	98.77	1	
Proposed method	97.53	2	17.45 ± 11.03 pixels

The images of DRIONS-DB (2047 × 1760) is larger than DRIONS-DB (600 × 400). Thus, the OD localization error is less in the latter case. In terms of accuracy and localization error, the proposed method achieves better results than the existing method in E-OPHTHA-EX, MESSIDOR, and DIARETDB1 (Tables 3–5). For remaining databases, we achieve comparable performance measures as the existing methods (Tables 6–10). The difference in OD localization errors between the existing methods and proposed method is only (1–2) pixels for DRIVE, STARE, ROC, DIARETDB0, STARE (Tables 6–10). This small difference may be due the variations in annotating the groundtruth. The proposed method is not able to exactly localize the OD center in 10 images (MESSIDOR, ROC, DIARETDB0 and STARE) and the images are shown in Fig. 12. Such failure cases arise mostly due to poor quality and missing of major blood vessels in the retinal image during acquisition and segmentation step.

Altogether, the proposed method is tested on 1978 images which include 1162 pathological images with different imaging environment, size, and field of view. The proposed method achieves an average OD detection accuracy of 99.49% computed for all databases. Our OD localization scheme is implemented in MATLAB environment running on a desktop computer (Intel Core i5, 3.4 GHz CPU and 4 GB RAM) and has an average computation time of 56 s per image. However, the timing can be improved significantly using optimized MATLAB code along with parallel processing implementation.

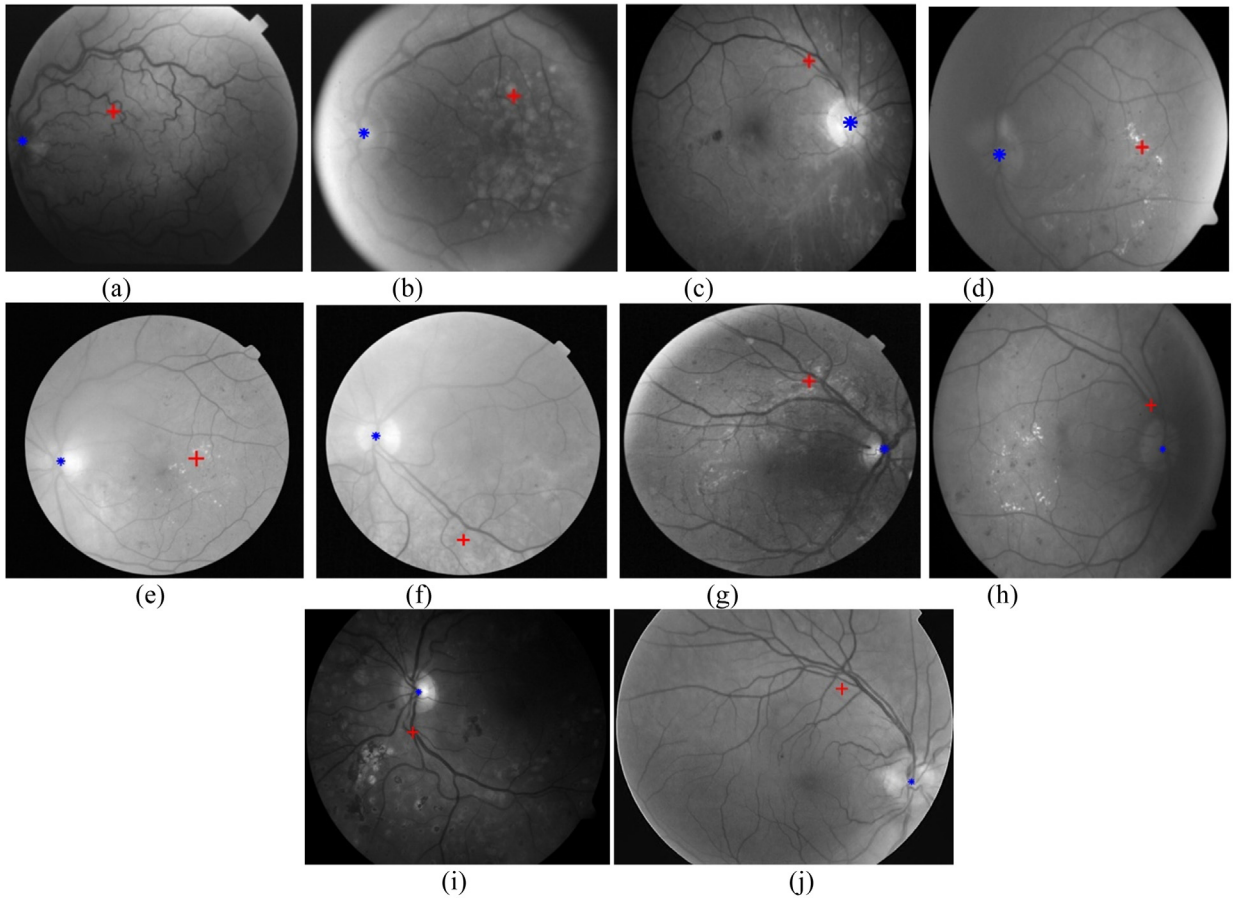

Fig. 12 – Examples of inaccurate of OD localization (detected OD center is labeled with "+", groundtruth as '*').

4. Conclusion

In this paper, a new method for accurate OD localization by incorporating three retinal vasculature based visual cues is presented. The visual cues such as global symmetry of vessel map, vessel component count and local symmetric vessel distribution inside the OD region are quantified. The proposed method is robust to OD appearance variation primarily arising due to pathological disorders. We extensively evaluated the new method using ten standard retinal databases out of which 1162 images include different stages of retinopathies. The proposed method successfully performed accurate OD center detection with 99.49% average accuracy. The new methodology is shown to be highly accurate which guarantees stability in OD detection irrespective of the acuteness of pathologies or image modality variation. The experimental results indicate that the proposed method can achieve state-of-the-art OD center localization error in challenging test cases.

REFERENCES

[1] Mookiah MRK, Acharya UR, Chua CK, Lim CM, Ng EYK, Laude A. Computer-aided diagnosis of diabetic retinopathy: a review. Comput Biol Med 2013;43(12):2136–55.

[2] Muramatsu C, Nakagawa T, Sawada A, Hatanaka Y, Hara T, Yamamoto T, et al. Automated segmentation of optic disc region on retinal fundus photographs: comparison of contour modeling and pixel classification methods. Comput Methods Programs Biomed 2011;101(1):23–32.

[3] Banerjee S, Kayal D. Detection of hard exudates using mean shift and normalized cut method. Biocybern Biomed Eng 2016;36(4):679–85.

[4] Sinthanayothin C, Boyce JF, Cook HL, Williamson TH. Automated localisation of the optic disk, fovea, and retinal blood vessels from digital colour fundus images. Br J Ophthalmol 1999;83(8):902–10.

[5] Walter T, Klein JC. Segmentation of color fundus images of the human retina: detection of the optic disc and the vascular tree using morphological techniques. Proc 2nd Int Symp Med Data Anal. 2001. pp. 282–7.

[6] Lu S, Lim JH. Automatic optic disc detection from retinal images by a line operator. IEEE Trans Biomed Eng 2011;58 (1):88–94.

[7] Hoover A, Goldbaum M. Locating the optic nerve in a retinal image using the fuzzy convergence of the blood vessels. IEEE Trans Med Imaging 2003;22(8):951–8.

[8] Foracchia M, Grisan E, Ruggeri A. Detection of optic disc in retinal images by means of a geometrical model of vessel structure. IEEE Trans Med Imaging 2004;23(10):1189–95.

[9] Youssif A, Ghalwash A, Ghoneim A. Optic disc detection from normalized digital fundus images by means of a vessels' direction matched filter. IEEE Trans Med Imaging 2008;27(1):11–8.

[10] Mahfouz A, Fahmy A. Fast localization of the optic disc using projection of image features. IEEE Trans Image Process 2010;19(12):3285–9.

[11] Lu S. Accurate and efficient optic disc detection and segmentation by a circular transformation. IEEE Trans Med Imaging 2011;30(12):2126–33.

[12] Welfer D, Scharcanski J, Kitamura CM, Pizzol MMD, Ludwig LWB, Marinho DR. Segmentation of the optic disk in color eye fundus images using an adaptive morphological approach. Comput Biol Med 2010;40(2):124–37.

[13] Soares IG, Castelo-Branco M, Pinheiro AMG. Optic disk localization in retinal images based on cumulative sum fields. IEEE J Biomed Health Inform 2016;20(2):574–85.

[14] Zhang D, Zhao Y. Novel accurate and fast optic disc detection in retinal images with vessel distribution and directional characteristics. IEEE J Biomed Health Inform 2014;20(1):333–42.

[15] Marino C, Penedo MG, Penas M, Carreira MJ, Gonzalez F. Personal authentication using digital retinal images. Pattern Anal Appl 2006;9(1):21–33.

[16] Panda R, Puhan NB, Panda G. New binary Hausdorff symmetry measure based seeded region growing for retinal vessel segmentation. Biocybern Biomed Eng 2016;36(1):119–29.

[17] GeethaRamani R, Balasubramanian L. Retinal blood vessel segmentation employing image processing and data mining techniques for computerized retinal image analysis. Biocybern Biomed Eng 2016;36(1):102–18.

[18] Panda R, Puhan NB, Panda G. Global vessel symmetry for optic disc detection in retinal images. IEEE National Conference on Computer Vision, Pattern Recognition, Image Processing and Graphics (NCVPRIPG). 2015. pp. 1–4.

[19] Huttenlocher DP, Klanderman GA, Rucklidge WA. Comparing images using the Hausdorff distance. IEEE Trans Pattern Anal Mach Intell 1993;15(9):850–63.

[20] Sudha N, Puhan NB, Xia H, Jiang X. Iris recognition on edge maps. IET Comput Vis 2009;3(1):1–7.

[21] Shonkwiler R. An image algorithm for computing the Hausdorff distance efficiently in linear time. Inform Process Lett 1989;30:87–9.

[22] Sivaswamy J, Krishnadas SR, Joshi GD, Jain M, Tabish S, Ujjwal. Drishti-GS: retinal image dataset for optic nerve head (ONH) segmentation. IEEE 11th International Symposium on Biomedical Imaging (ISBI). 2014. pp. 53–6.

[23] Carmona EJ, Rincón M, García-Feijoo J, Martínez-de-la-Casa M. Identification of the optic nerve head with genetic algorithms. Artif Intell Med 2008;43(3):243–59.

[24] Decencire E, Cazuguel G, Zhang X, Thibault G, Klein JC, Meyer F, et al. Teleophta: machine learning and image processing methods for teleophthalmology. IRBM 2013;34 (2):196–203.

[25] MESSIDOR. Digital retinal images. Online available from: http://messidor.crihan.fr/download-en.php.

[26] Kalesnykiene V, Kamarainen JK, Voutilainen R, Pietil J, Klviinen H, Uusitalo H. Diaretdb1 diabetic retinopathy database and evaluation protocol; 2014.

[27] Kalesnykiene V, Kamarainen J, Lensu L, Sorri I, Uusitalo H, Klviinen H, et al. Diaretdb0: evaluation database and methodology for diabetic retinopathy algorithms. Finland: Machine Vision and Pattern Recognition Research Group, Lappeenranta University of Technology; 2006.

[28] Staal J, Abramoff M, Niemeijer M, Viergever M, Ginneken BV. Ridge-based vessel segmentation in color images of the retina. IEEE Trans Med Imaging 2004;23(4):501–9.

[29] Odstrcilik J, Kolar R, Budai A, Hornegger J, Jan J, Gazarek J, et al. Retinal vessel segmentation by improved matched filtering: evaluation on a new high-resolution fundus image database. IET Image Process 2013;7(4):373–83.

[30] Niemeijer M, Ginneken BV, Cree M, Mizutani A, Quellec G, Sanchez C, et al. Retinopathy online challenge: automatic detection of microaneurysms in digital color fundus photographs. IEEE Trans Med Imaging 2010;29(1):185–95.

[31] Hoover AD, Kouznetsova V, Goldbaum M. Locating blood vessels in retinal images by piecewise threshold probing of a matched filter response. IEEE Trans Med Imaging 2000;19 (3):203–10.

[32] Aquino A, Gegundez ME, Marin D. Automated optic disc detection in retinal images of patients with diabetic retinopathy and risk of macular edema. Int J Biol Life Sci 2010;8(11):87–92.
[33] Ramakanth SA, Babu RV. Approximate nearest neighbour field based optic disk detection. Comput Med Imaging Graph 2014;38(1):49–56.
[34] Franklin SW, Rajan SE. Computerized screening of diabetic retinopathy employing blood vessel segmentation in retinal images. Biocybern Biomed Eng 2014;34(2):117–24.
[35] Giachetti A, Ballerini L, Trucco E, Wilson PJ. The use of radial symmetry to localize retinal landmarks. Comput Med Imaging Graph 2013;37(5):369–76.
[36] Bekkers E, Loog M, Romeny BH, Duits R. Template matching via densities on the roto-translation group. IEEE Transactions on Pattern Analysis and Machine Intelligence; 2017.
[37] Dashtbozorg B, Mendonça AM, Campilho A. Optic disc segmentation using the sliding band filter. Comput Biol Med 2015;56:1–12.